



Pyroclastic density currents (PDC) of the 16–17 August 2006 eruptions of Tungurahua volcano, Ecuador: Geophysical registry and characteristics



Minard L. Hall ^{*}, Alexander L. Steele, Patricia A. Mothes, Mario C. Ruiz

Instituto Geofísico, Escuela Politécnica Nacional, Quito, Ecuador

ARTICLE INFO

Article history:

Received 3 February 2013

Accepted 28 August 2013

Available online 4 September 2013

Keywords:

Tungurahua

Ecuador

2006 eruption chronology

Instrumental monitoring

PDC characteristics

ABSTRACT

Tungurahua, located in the Eastern Cordillera of the Ecuadorian Andes, is a 5023 m-high active volcano, notable for its extreme relief (3200 m), steep sides, and frequent eruptive cycles. From 1999 until 2006 Tungurahua experienced short periods of low to moderate strombolian activity, characterized by fire fountaining, explosions, frequent ash falls and debris flows, and no PDC events. Without warning, Tungurahua initiated PDC activity on 15–16 July 2006, which became more intense on the night of 16–17 August 2006, which is the focus of this study. Continuous monitoring of Tungurahua has employed seismic (both short period and broadband (BB) instruments), SO₂ gas emission (COSPEC and DOAS), and geodetic methods (EDM, tilt meters, and GPS), in addition to thermal imagery (airborne and ground-based). Acoustic flow monitors (AFM) installed to monitor lahar activity were important for detecting PDC events. Acoustic signals were monitored at Riobamba, 40 km to the SW, as well as by infrasound sensors at Tungurahua's BB seismic stations.

Based on geophysical parameters, visual observations, and PDC deposit characteristics, four phases of distinct eruptive activity are recognized during the 16–17 August episode. Phase I (08H37 to 21H13 of 16 Aug.) (local time) experienced low to moderate strombolian activity with occasional high energy impulsive bursts and small PDC. Phase II (21H13–16 Aug. to 00H12–17 Aug.) was characterized by a number of discrete events with high amplitude seismo-acoustic signals, followed by the generation of larger PDC that overran monitoring stations and had velocities of 30–33 m/s. After midnight, Phase III (00H12 to 01H14) saw an intense period of unrelenting eruptive activity corresponding to the episode's greatest energy release. It was characterized by subplinian activity accompanied by a series of high energy outbursts and constant low frequency jetting that together formed a continuous plume. It was during this phase that the largest PDC were produced, reaching the surrounding river valleys. Phase IV (after 01H14) followed the cessation of the paroxysmal eruption, but witnessed many granular PDC generated by degassed lava spill outs from the crater that developed lobe and channel morphology on the cone's lower flanks. Hours later a blocky lava flow issued from the crater.

During these episodes, more than 30 PDC events were detected, the majority being small flows that remained high on the cone. The two largest PDC occurred after midnight, probably generated by fountain collapse. Their descent down the cone's upper steep flanks (~28°) and 2.4 km in length favored air entrainment, resulting in PDC with greater fluidity. These flows had volumes of 9 to 17 × 10⁶ m³ and produced widespread, but relatively thin (1–2 m thick) normally-graded deposits at their distal ends. The character and evolution of the PDC activity apparently reflect decreasing volatile contents of the magma and a diminishing magma supply.

© 2013 Elsevier B.V. All rights reserved.

1. Introduction

Tungurahua volcano (lat. 01°28'S; long. 78°27'W) is located in the Eastern Cordillera of the Ecuadorian Andes, 120 km south of Quito and 33 km southeast of Ambato, the capital of Tungurahua Province. This 5023 m-high active volcano is notable for its extreme relief (3200 m), steep sides, and frequent eruptive cycles; its 400 m-wide crater, situated slightly NW of Tungurahua's summit, has its lower rim (4770 m) also on its NW side. Along with other large active stratovolcanoes such as Cotopaxi, Sangay, Antisana and Cayambe, it defines the eastern row of

andesitic volcanoes in Ecuador, some 35 km behind the volcanic front in the Western Cordillera (Hall et al., 2008).

Five eruptive episodes of Tungurahua have been reported in historic and recent documents: in 1641–46, 1773–81, 1886–88, 1916–18, and the 1999-to-present episode (Hall et al., 1999; Le Pennec et al., 2008). Lava emissions, pyroclastic flows, ash falls, and debris flows characterize this volcano's activity. As such, Tungurahua is considered to be a dangerous volcano which potentially threatens the town of Baños (residents ~20k daily; visitors ~50k on holidays), as well as other small villages located on its flanks (Fig. 1) (Hall et al., 2002). The Agoyan hydroelectric plant, the second largest in Ecuador, is only 7 km down the Pastaza River from the volcano. This paper documents the development and culmination of PDC activity associated with the 16–17 August

^{*} Corresponding author.

E-mail address: volcan_pete@yahoo.com (M.L. Hall).

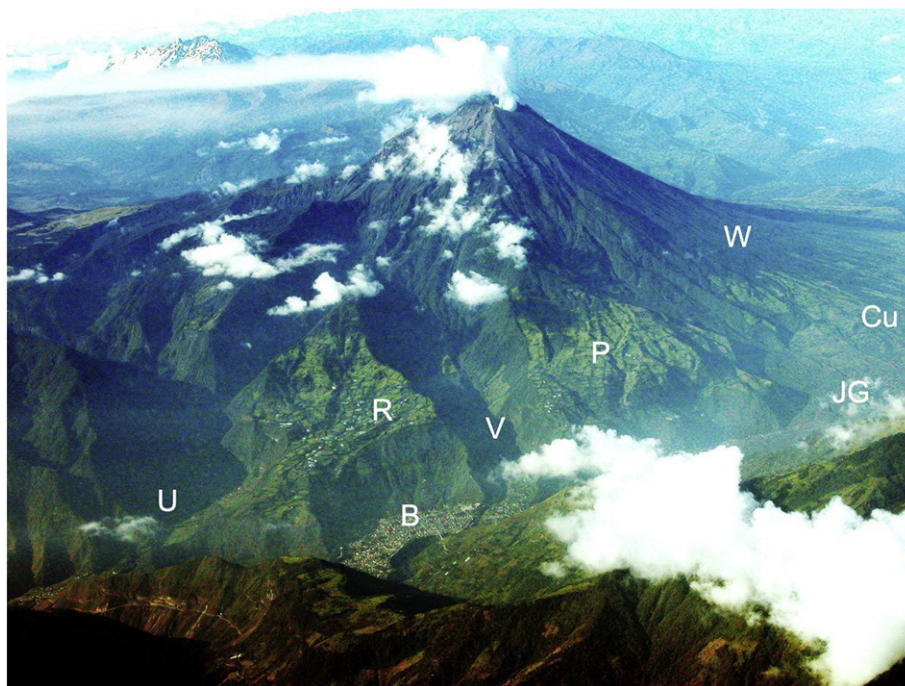


Fig. 1. View of Tungurahua (5023 m) as seen from the north. Baños (1800 m) with its 20k inhabitants in foreground. Important sites include: U – Ulba valley, B – Baños city, R – Runtun village, V – Vascún valley, P – Pondoá village, JG – Juive Grande valley, Cu – Cusúa village, W – Northwest and west flanks of Tungurahua cone. See also Fig. 2.

2006 eruption, especially its timing, its associated seismic and infrasound signals, its spatial distribution, and its deposit characteristics. Kelfoun et al. (2009) employed many parameters of this eruption for modeling experiments of PDC.

Beginning in 1998 and continuing in early 1999, an intermittent series of VT and LP seismic swarms was detected by the monitoring net of the Instituto Geofísico (IG) of the Escuela Politécnica Nacional in Quito that suggested a possible reawakening of Tungurahua. Anomalous seismic activity returned in May 1999 and intensified in September and October 1999 (Mothes et al., 2004). Mountain guides reported elevated fumarolic activity in the crater in late July 1999. The first COSPEC SO₂ measurements in late August 1999 registered values of 2300 tons/day which ascended to 10,000 tons/days in October 1999 (Arellano et al., 2008). This was accompanied by mild strombolian activity with the eruption of incandescent blocks and light ash falls that lasted only a few weeks.

From 1999 until 2006 Tungurahua had periods of low to intermittent activity, characterized by strombolian and rare vulcanian episodes of varying intensities. The periodic strombolian activity was characterized by frequent explosions, fire fountaining, ejected incandescent blocks, frequent ash falls and debris flows, but no PDC activity. Vulcanian events accompanied the more intense strombolian eruptions and were characterized by very large explosions with high acoustic amplitudes and powerful audio booms (Ruiz et al., 2006). PDC events were first observed in 14–16 July, but these were greatly surpassed in frequency and volume in the 16–17 August episode. During this 7 year period, as well as in the past several centuries, Tungurahua's andesites have typically been comprised of 58–59% SiO₂ (Samaniego et al., 2011), the exception being rare dacitic outbreaks.

Since Tungurahua's reactivation in 1999, the IG has maintained 24 h/day monitoring at its observatory (OVT), 15 km NNW of the crater, as well as at its principal office in Quito. Continual monitoring of Tungurahua has employed seismic (both short period and broadband (BB) instruments), SO₂ gas emission (COSPEC and DOAS), and geodetic methods (EDM, tilt meters, and GPS). In addition thermal imagery (airborne and ground-based) has been available for the past 10 years, which has proven to be invaluable for night and bad weather observations. Acoustic flow monitors (AFM) established on the cone to monitor

lahar activity were important for detecting PDC events. Given that there was no rainfall in the area in 16–17 August, all AFM events were interpreted to be PDC events. Infrasound sensors located in Riobamba, 40 km to the SW (Garcés et al., 2008), as well as those at Tungurahua's BB seismic stations also aided in pinpointing the exact time and estimating the magnitude of the eruptive events (Kumagai et al., 2010).

The main eruptions occurred between 21H13 (16 Aug.) and 01H14 (17 Aug.) (all local times = EST of USA). The increasing PDC activity was observed first by seismic and visual monitoring, then by night-vision monocular, video filming, and thermal imagery, all recorded at OVT. Critical visual observations were made and radioed to OVT by local inhabitants/observers in real time. Additional satellite and infrasound data were obtained from Fee et al. (2010) and Steffke et al. (2010).

The largest PDC that arrived at the foot of the volcano were registered by their abrupt loss-of-signal times of impacted monitoring instruments, or by the high frequency signals recorded by seismic and AFM sensors as the PDC passed nearby, and by direct observation. The steep flanks (~28°) of the cone and the subsequent channeling of the PDC in narrow ravines that descend the intermediate and lower flanks of the edifice permitted the largest flows to reach the surrounding river valleys, 7–8 km distant, on the S, SW, W, and NW sides of the volcano (Fig. 2). In total ≥30 PDC flows were detected during the 16–17 August episode, the majority being small flows that remained high on the cone (Barba et al., 2006). Because the amplitudes of seismic tremor were constantly increasing during the morning of 16 August and knowing that the earlier July eruption had generated the first pyroclastic flows of the 1999–2006 cycle, at about 10 am of 16 August the IG recommended the immediate evacuation of the volcano's flanks, which began shortly thereafter and was finished by late afternoon. However, Baños' officials decided to ignore the warning and the evacuation of Baños was left to individual discretion.

2. Chronology of events related to the main PDC activity

After the eruption of 14–16 July 2006, Tungurahua's volcanic activity decreased dramatically and had all but ceased by 26 July. However, by 29 July activity resumed with the initiation of short-duration, small amplitude seismic signals, which had increased to >300 events/day by 9

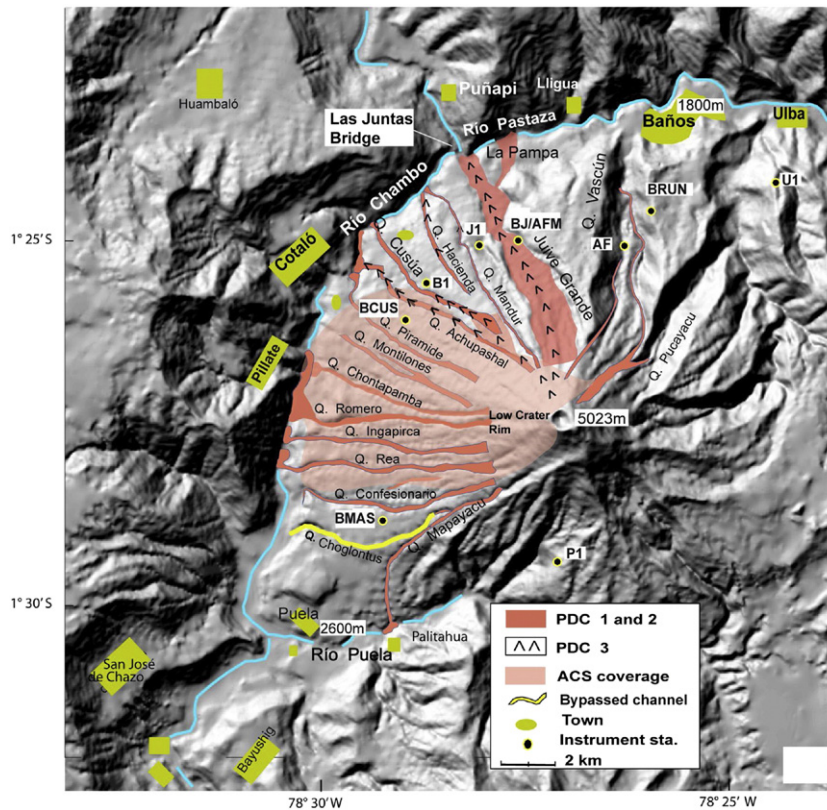


Fig. 2. Digital elevation model displaying the main quebradas (ravines) used by the PDC from the crater and the PDC deposits blocking the Chambo river valley (darker red). Thicker ash cloud surge deposits shown in pink. Broad-band stations: BMAS, BCUS, BRUN, and BJ. Short period seismic stat.: B1, J1, P1, and U1. AFM stat: BJ/AFM and AF (Vascún).

August. Long period (LP) seismic events, interpreted as movement of magma at depth, accompanied these signals.

At 08H37 on 16 August 2006, two volcano-tectonic (VT) quakes located at <5 km depth beneath Tungurahua's summit marked the beginning of the 16–17 August eruptive cycle, which we divide into four phases based on seismo-acoustic amplitudes and energy registered by three BB seismic and infrasound stations (BCUS, BMAS, and BRUN) whose data are preferentially used here (Fig. 2). Seismic amplitudes are expressed as Seismic Reduced Displacement (SRD) in cm^2 . Displacement values for each discrete event recorded by the three BB stations are normalized to the source location (vent), and then an averaged SRD is calculated by taking the mean amplitude between the station's values. Acoustic amplitudes, expressed as Infrasound Reduced Pressure (IRP) and given in Pascals (Pa) for the same three stations, are normalized to 1 km from the vent, and then an averaged value calculated. Seismic and acoustic energies given in Joules (J) are representative of energy release at the vent, as perceived by individual stations. Only averaged seismic and acoustic energies between the three stations are given, but are calculated for both discrete events and for five-minute windows beginning with the event's onset (Table 1).

Discrete seismic outbursts were selected based on signal amplitude, then filtered between frequencies in the 0.2 to 10 Hz bandwidth. However, during large segments of the observation period, particularly during the paroxysmal phase of the midnight eruptions, the seismic and infrasound registry was too saturated and complex to discern the majority of individual events (Figs. 3 and 4). As such, only significant discrete outbursts, verified by visual observation and discernible in the seismic and acoustic records, are studied here and listed in Table 1.

It is important to emphasize that most nearby observers perceived and described the discrete seismo-acoustic outbursts during Phases I and II as very large “vulcanian” explosions (Barba et al., 2006). However, careful filtering of the outburst infrasound traces reveals that they do not display typical explosion waveform characteristics, comprised of discrete, short-duration signals with an impulsive acoustic onset and

an N-shaped waveform (Morrissey and Mastin, 2000; Johnson and Ripepe, 2011). Fee et al. (2010) note that explosion waveforms at Tungurahua during the 16–17 August 2006 eruptions were often difficult to discern due to the interference of other signals, primarily a continuous ~5 Pa peak-to-peak jetting. While we conclude that the majority of the bursts during phases I and II were likely vulcanian explosions, due to the lack of seismic and acoustic waveform evidence we refer to these events as discrete high-energy outbursts of activity. In Phase III observers also described vulcanian-like outbursts during the continuous subplinian activity, however we refer to these as discrete high energy spikes within a subplinian regime, as we imagine that we are dealing with an open vent system at this time.

Phase I of the 16–17 August eruptive cycle started at 08H37 in 16 August, lasted until 21H13, and consisted of low to moderate strombolian activity (Table 1). Four distinct eruptive outbursts during this phase had averaged SRD values of 6.4 cm^2 to 213 cm^2 . Also near and distal seismic stations of the IG's regional network began registering large amplitude, mixed harmonic and spasmodic volcanic tremor. At 10H00 ash emission became more intense, resulting in a 1.5 km-high column that traveled to the west. Volcanic tremor increased notably at 14H30, producing strong vibrations felt all around the cone. One very strong outburst at 14H43 caused a notable spike in the infrasound registry at BCUS station (Fig. 5B). At 15H15 an ash-charged plume lofted to 2.25 km above the volcano and was detected by a GOES satellite (Steffke et al., 2010).

Small pyroclastic flows began descending Tungurahua's upper NW-W flanks above Cusúa village at about 16H50 (Barba et al., 2006), recorded by a seismic signal with a 137 cm^2 amplitude. Lava fountaining intensified after 17H10 and with nightfall the cone became totally incandescent as mobile rugs of red ejecta rolled down the upper flanks. Most inhabitants of the surrounding villages were evacuated by 18H00, the exception being Baños city.

Phase II started at 21H13 and consisted of ~3 h of increasing lava fountaining punctuated by discrete, highly energetic eruptive events whose average SRD values ranged from 223 cm^2 to 730 cm^2 . IRP values

Table 1
 Chronological listing of discrete seismic outburst events recorded by seismo-acoustic monitoring stations, often verified by visual observations. Values of seismic amplitude as Seismic Reduced Displacement (SRD; cm²) and acoustic amplitude as Infrasound Reduced Pressure (IRP; Pa) are given for each event, as registered by each of the three broadband seismic/infrasound stations. SRD values are normalized to a distance of 1 km from the vent. An averaged seismic and acoustic amplitude value from the three BB stations is also given. Averaged seismic and acoustic energies (Joules; J) from the three BB stations are normalized to the source (vent) and are specified for discrete events as well as for 5-minute windows, starting with event onset.

Event Date & Time			Seismic & Acoustic Amplitude						Seismic & Acoustic Energy				TABLE 1			
Event No.	E Date (UTC)	E Time (UTC)	BCUS		BMAS		BRUN		Averaged Seismic Amplitude (/no. STNs) ^a	Averaged Acoustic Amplitude (/no. STNs)	Averaged Seismic Energy (/no. STNs)	Averaged Acoustic Energy (/no. STNs)	Averaged Seismic Energy (Joules*) (/no. STNs)	Averaged Acoustic Energy (Joules*) (/no. STNs)	Local Observations & Published Reports	
			SRD (cm ²)	IRP (Pa)	SRD (cm ²)	IRP (Pa)	SRD (cm ²)	IRP (Pa)								SRD (cm ²)
Phase I																
1	08/16/06	13H37	08H37	7.51	37.95	6.21	10.74	5.36	19.87	22.86	1.97E+05	1.93E+06	7.03E+06	1.49E+07	Initiation of wide-amplitude harmonic & spasmodic tremor. Low to moderate Strombolian activity. First sight of small PDC's flowing down west flank. Lava fountaining 800 m above crater rim.	
2	08/16/06	19H43	14H43	217.93	521.76	130.94	209.61	125.85	368.77	366.71	1.39E+08	6.03E+08	3.43E+08	1.56E+09		
3	08/16/06	21H51	16H51	189.14	200.94	120.12	67.19	100.53	203.94	157.35	1.08E+08	5.96E+08	2.03E+08	1.06E+09		
4	08/17/06	00H49	19H49	304.95	389.89	180.64	212.75	153.09	202.28	212.89	1.70E+08	5.75E+08	9.96E+08	3.45E+09		
Phase II																
5	08/17/06	02H13	21H13	1304.53	454.60	461.49	217.62	424.87	233.63	301.95	4.96E+09	2.33E+09	7.30E+09	7.88E+09	Series of strong outbursts with wide amplitudes followed by PDC transport tremor. PDC without outburst. (Achuaphashal Q.) BCUS telemetry cut. Juive Grande AFM registers PDC event. PDC's arrive to Chambo river. All local short-period seismic stations saturated. Distal stations (100 km) register 1–2 cm signal amplitude. PDC in upper Vascun Quebrada; PDC in Mandur Q. Juive AFM registers PDC; PDC in Q. Hacienda Lava fountain rises 1500 m above crater rim. PDC's dam Chambo river. Reports of very loud, strong explosions heard at OVT and Pillate.	
6	08/17/06	02H25	21H25	305.47	257.96	205.78	142.09	157.25	193.09	197.71	5.74E+08	1.29E+09	1.27E+09	3.24E+09		
7	08/17/06	02H43	21H43	1127.57	449.75	413.64	247.60	429.69	214.53	303.96	3.34E+09	2.60E+09	5.58E+09	8.54E+09		
8	08/17/06	02H57	21H57	407.54	370.66	269.05	169.02	214.13	256.58	265.42	3.70E+08	1.57E+09	2.01E+09	7.92E+09		
9	08/17/06	03H15	22H15	496.39	447.48	343.89	319.07	262.77	271.47	346.01	1.02E+09	3.80E+09	2.56E+09	9.23E+09		
10	08/17/06	03H30	22H30	506.14	352.49	334.19	213.15	224.58	310.31	291.98	2.22E+09	5.40E+09	3.10E+09	7.78E+09		
11	08/17/06	04H12	23H12	497.87	587.98	342.68	228.81	233.08	262.69	359.83	2.29E+09	9.43E+09	2.70E+09	1.09E+10		
12	08/17/06	04H52	23H52	452.57	161.60	289.33	81.88	213.42	259.08	167.50	9.80E+08	1.88E+09	2.49E+09	3.60E+09		
13	08/17/06	05H02	00H02	453.26	202.15	283.71	120.14	219.93	342.35	221.55	2.09E+09	3.55E+09	2.37E+09	3.94E+09		
Phase III																
14	08/17/06	05H12	00H12	566.61	164.21	268.11	75.80	198.38	252.37	164.13	5.89E+09	2.53E+09	7.82E+09	3.64E+09		Increase of PDC activity on NW flanks. PDC's reported down SW flanks – Puela affected. PDC-1 generated. Electrical TX cut. Baños without electricity. PDC-2 generated. BCUS infrasound sensor damaged. Elevated lava fountaining. BMAS station transmission cut (00h46m). PDC's on W-SW flanks – implied by BMAS seismic trace. Numerous reports of lapilli fall at Juive, Puela & Ambato. BMAS infrasound sensor damaged at 01h02m. Energetic activity ends. End of Phase III. PDC-3 series begins. No notable discrete seismic events registered, only tremor.
15	08/17/06	05H20	00H20	690.32	306.69	350.56	116.37	220.07	252.33	225.13	7.19E+09	3.47E+09	1.32E+10	2.73E+10		
16	08/17/06	05H24	00H24	1074.90	*NaN	383.62	112.53	236.36	270.16	191.34	3.18E+10	4.11E+09	3.98E+10	5.94E+09		
17	08/17/06	05H32	00H32	1084.45	NaN	589.98	94.77	287.67	417.80	208.90	3.17E+10	9.11E+09	3.92E+10	1.15E+10		
18	08/17/06	05H37	00H37	1236.95	NaN	547.65	97.20	335.68	396.77	246.99	3.65E+10	9.94E+09	4.94E+10	1.37E+10		
19	08/17/06	05H49	00H49	1322.62	NaN	823.86	297.10	417.35	414.16	355.63	4.04E+10	1.03E+10	6.53E+10	1.80E+10		
20	08/17/06	06H06	01H06	931.63	NaN	620.59	NaN	344.18	383.28	383.28	1.44E+10	1.79E+10	2.15E+10	2.25E+10		
21	08/17/06	06H14	01H14	635.76	NaN	316.58	NaN	296.71	270.00	270.00	1.75E+09	6.59E+09	1.93E+09	8.97E+09		
Phase IV																

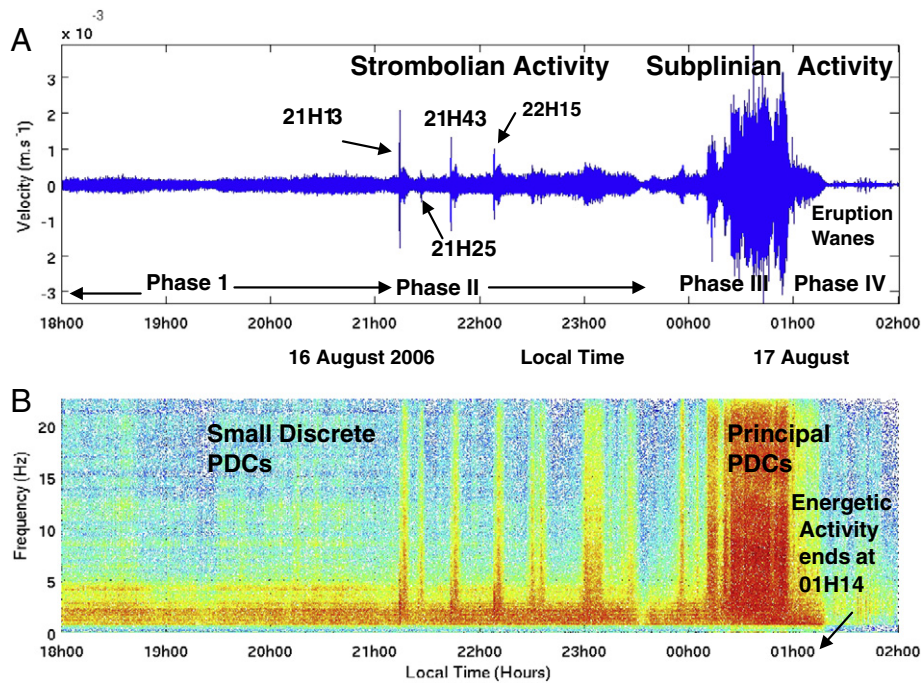


Fig. 3. (A) Seismic trace registered at BCUS BB seismic station from 18H00 16 August to 02H00 17 August. The four phases of the eruptive episode are indicated. In Phase II, eruptive outbursts and subsequent tremor representing PDC transport are indicated at 21H13, 21H43, and 22H15. (B) Spectrogram for the same time interval representing seismic outbursts and PDC sequences as shown by their frequency (Hz) ranges.

averaged 168–360 Pa at the three stations (Table 1; Fig. 5B). Overall, seismic energy output in Phase II averaged an order of magnitude higher than that of Phase I. Between 21H13 and 00H02 (17 Aug.) nine high energy outbursts transpired (21H13, 21H25, 21H43, 21H57, 22H15, 22H30, 23H12, 23H52 and 00H02), of which three events (21H13, 21H43 and 22H15) produced PDC that descended the Cusúa-Achupashal drainages and were recorded at BCUS station (Fig. 3). These events had averaged SRD values of 730, 657, and 368 cm², respectively, and averaged IRP values between 302 and 346 Pa (Table 1). The predominant pattern observed in each of these three events consisted of a large seismic outburst signal, followed ~150 s later by a high

frequency tremor (10–20 Hz) registered at BCUS, assumed to be a passing PDC (Fig. 3A, B). Noteworthy is the 21H25 event that marks the passage of a PDC and the cutting of the BCUS telemetry. This PDC is not associated with any impulsive outburst event, suggesting that it might have originated by the sluffing off of accumulated ejecta from the crater's edge.

Four discrete eruptive outbursts registered between 22H30 and 00H02 (17 Aug.) had averaged SRD levels of about 340 cm². The energetic 23H12 outburst expelled considerable lithic material which generated a large PDC that descended the JG valley ($V = 6.9$ m/s) and was registered by the Juive AFM station. Several PDC had enough

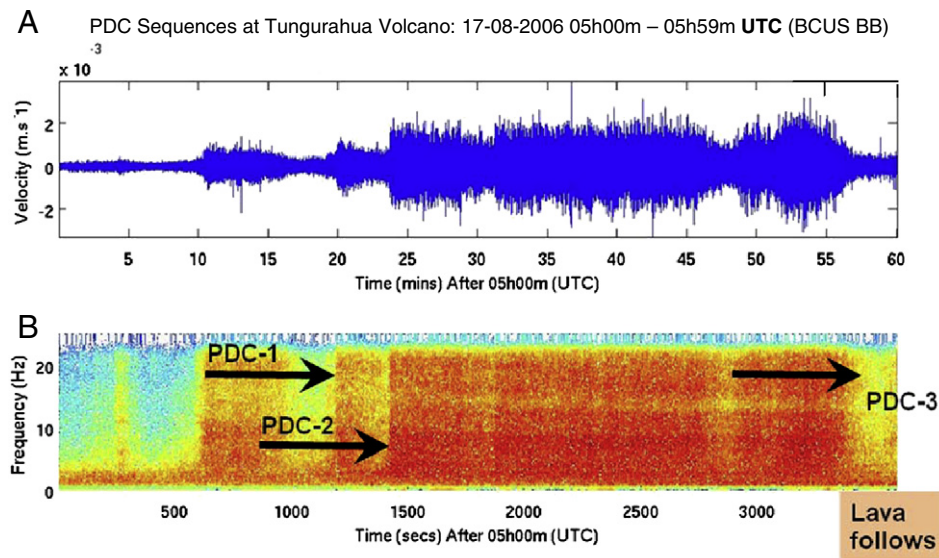


Fig. 4. (A) An expanded seismic trace from BCUS BB seismic station during Phase III (05H00 to 05H59 17 August (UTC), that is, 00H00 to 00H59 17 August (local time)). Continuous and saturated seismic outbursts obscure the presence of discrete eruptive events. (B) A spectrogram for the same time period clearly indicates the major outbursts which were also confirmed by visual sighting. The important PDC discussed in this paper are indicated by arrows.

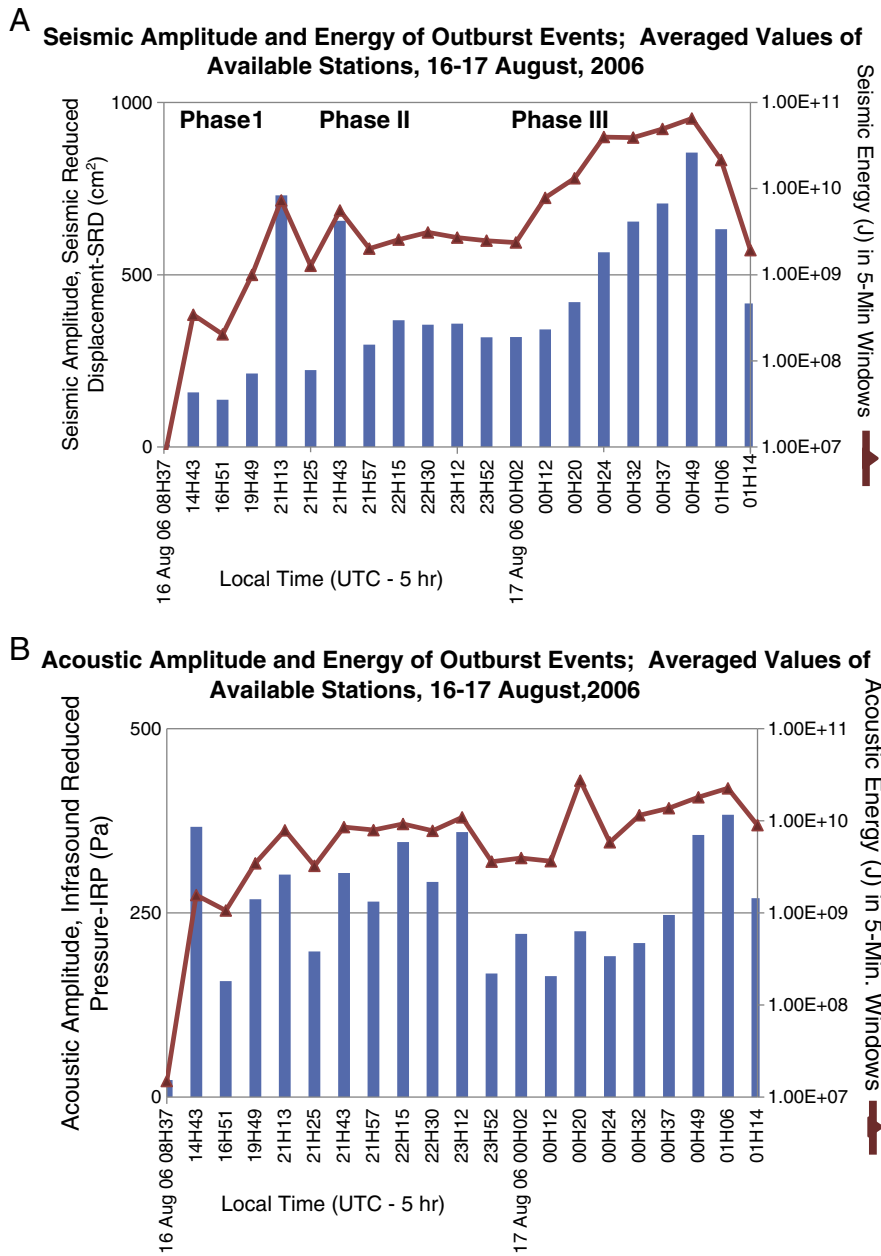


Fig. 5. Bar graphs displaying (A) averaged seismic amplitudes as Seismic Reduced Displacement (SRD; cm²) of discrete outburst events registered by the three BB seismic stations. Values are normalized to the source (vent). The dark line with triangles represents the averaged seismic energy release (Joules; J) calculated for 5-minute windows after event onset. Values are normalized to the source (vent). The seismic energy accumulated over a 5-minute window is considerably higher than values for discrete events, since they include registry of subsequent PDC and lava fountaining. (B) Averaged acoustic amplitudes as Infrasonic Reduced Pressure (IRP; Pa) of discrete outburst events registered by infrasound sensors at the same BB stations and normalized to 1 km from the vent. Averaged acoustic energy, expressed in Joules (J) for 5-minute windows after discrete event onset, is also indicated; its values are elevated, since they include perturbations by almost continual lava fountaining and PDC activity.

volume to reach and dam the Chambo river whose typical water discharge had been ~40 m³/s. Local observers confirmed that the Chambo river was dammed at the Achupashal confluence by 23H42.

Until midnight the eruption style was typically strong to violent strombolian, characterized by constant lava fountaining, mild ash falls, occasional higher energy outbursts, and moderate PDC activity down the cone's western side. As seen in GOES imagery, plume heights increased markedly during this phase and reached 6.5 to 8.25 km above the crater rim (Steffke et al., 2010). Infrasound instruments in Riobamba registered levels up to 10 MW at about 00H00 (17 August) (Fee et al., 2010).

Phase III involves the paroxysmal eruptions that transpired between 00H12 and 01H14 of 17 August (Fig. 4). This phase was dominated by constant fire fountaining and a continuous series of high energy

outbursts as well as a low frequency (<0.1 Hz) jetting (Fee et al., 2010). Kumagai et al. (2010) also note that increasing amplitude tremor occurred during this interval which was generated by both eruptions and PDC. While seismic and acoustic records were noisy and complex throughout this phase of the eruptive sequence, thus making it difficult to discern specific volcanic signals, distinct outbursts were visually observed and noted in the log book. We estimate that averaged SRD amplitude levels of these events reached their highest levels and remained above 400 cm² and often greater than 500 cm², notably higher than levels registered in Phase II (Fig. 4A).

At 00H12 and 00H20 two large seismic events (341 cm² and 420 cm²) resulted in PDC that descended the Cusúa and JG valleys, as well as the Mapayacu arroyo on the south flank, where it reached the Puela river for the first time (Fig. 2; Table 1). With the 00H20 event,

observers warned of the violent descent of large PDC in channels on the SW and NW flanks, the latter being where the JG BB seismic and AFM stations were overrun by a major flow, here labeled PDC-1, whose velocity was estimated at ~ 21 m/s based on the 4 min travel time provided by observers. Farther down valley it cut the electric power lines to Baños at 00H24, leaving the city without electricity. The same outburst sent a PDC down the eastern branch of Vascún valley, registered at 00H26 by its AFM station; this PDC stopped only 1 km upstream of the popular El Salado hot springs spa in Baños' western suburbs.

A larger eruptive outburst (565 cm^2) occurred at 00H24 (Fig. 4A) that generated PDC-2. It also descended the JG valley, destroying the 5 m-high ceramic bird statue “Los Pájaros”, near Las Juntas bridge at 00H28. It then dropped into the deep Pastaza canyon, dammed the river, but its surge climbed 30 m up the opposite canyon wall. A coeval flow in the Cusúa arroyo damaged the BCUS infrasound sensor.

By 00H30, Garcés et al. (2008) reported that the total acoustic power of the eruption had risen to 30 MW. However, by including the lower frequencies of <0.1 Hz, the total acoustic power is close to ~ 50 MW during this phase of the eruption (Steffke et al., 2010). At 00H33 OVT staff noted that the fire fountaining reached heights of 1–2 km above the crater rim and was accompanied by very loud “cañonazos”, interpreted to be vulcanian explosions (Barba et al., 2006). The cañonazos were associated with the high energy seismic outbursts registered at 00H32 and 00H37 by all BB stations (Table 1, Figs. 4A and 5A), which were followed by a widespread scoria lapilli fall beginning at 00H44 and possibly by PDC that destroyed the BMAS station's telemetry at 00H46. These two outbursts were associated with two large VLP (very long period) seismic events which Kumagai et al. (2010) located at ~ 3 km below the crater. They suggest that these events were associated with volumetric changes brought on by degassing processes in the deeper magma that resulted in bubble formation and growth, and to a more buoyant magma, thus facilitating its rapid ascent and the initiation of violent eruptions (Kumagai et al., 2010). In addition Samaniego et al. (2011) found evidence based on the size of rim overgrowths on plagioclase of a hotter mafic magma that had ascended from depth. This magma recharge likely contributed to magma degassing and a faster magma ascent rate that led to the Phase III paroxysmal eruptions. Wright et al. (2012) also identified a high magma supply rate for the August 2006 eruption and they show that the low concentration of crystals in the glass is the result of a fast magma ascent and a high supply rate ($1000 \text{ m}^3/\text{s}$). The very high energy of these events is corroborated by the fact that in the Puela area on Tungurahua's SW flank, blocks 22 cm in diameter were ejected ballistically out to 7.2 km from the vent and had initial velocities calculated at ~ 313 m/s (Arellano and Hall, 2007).

After 00H45, GOES imagery shows that the eruption plume had ascended to its maximum height of ~ 22.5 km and spread out to form a 156×134 km umbrella-shaped cloud (Steffke et al., 2010). At 00H49 PDC descended all main channels of the SW, W, and NW flanks, and overran JG's 1 Hz seismic station. The BMAS infrasound sensor was destroyed at 01H02, apparently by these PDC. SRD values of distinct outbursts continued to ascend through 00H49 and then began to decline (Figs. 4 and 5).

By 00H55 seismicity had essentially ended at Cusúa station, implying that PDC activity had finished there. However, PDC activity continued in the SW, most likely in the Mapayacu drainage, as strong seismic energy continued to be recorded until 01H14 by BMAS station. By 01H35 seismic traces of the surviving stations returned to near-background amplitudes and acoustic power had also dropped to near-background levels of 1.8×10^4 W (Steffke et al., 2010). It is presumed that the PDC-3 flows occurred sometime after 01H14, following the cessation of ash-forming outbursts, since the subsequent PDC-3 deposits have no ash cover.

It should be emphasized that the largest seismic outbursts of the entire eruptive period were those associated with the two VLP seismic

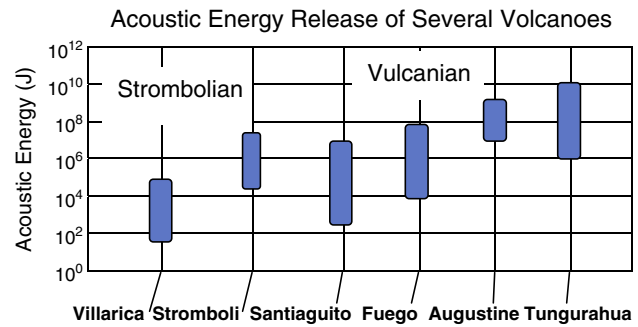


Fig. 6. Range of acoustic energy (J) registered at six volcanoes, representative of strombolian and vulcanian eruptive activity. Augustine data from Petersen et al. (2006); other data from Marchetti et al. (2009). Tungurahua's acoustic energy values, normalized to the source (vent) and averaged for the three BB stations, are equal to or greater than those of other well-documented vulcanian eruptions.

events of 00H32 and 00H37, and those at 00H49 and 01H06, each with average SRD values between 632 cm^2 and 855 cm^2 . Furthermore the principal discrete eruptive events had infrasound energies of 10^6 to 10^{10} J that are equivalent or greater than vulcanian explosions described at other volcanoes (Fig. 6).

Although mass flux rates for SO_2 emissions have not been scaled to Tungurahua's eruption intensity, it is noteworthy that the eruptions of 16–17 August emitted a total of 35,000 tons in ≤ 18 h, as compared to a daily average of ~ 1500 tons/day over the previous seven years, for a total of 3.8 million tons (Arellano et al., 2008).

3. Pyroclastic density currents (PDC)

3.1. Introduction

Intense PDC activity began at 21H13 (16 Aug.) and ended sometime after 01H14 (17 Aug.). Phase II witnessed continuous lava fountaining punctuated by occasional high energy outbursts that generated PDC. Phase III (00H12 to 01H14 of 17 Aug.) corresponds to intense subplinian activity of continuous high energy jetting of volcanic materials with occasional outbursts that generated the largest PDC events, two of which (PDC-1 and 2) are selected for further description. The large eruptive event at 00H20 generated PDC-1 that subsequently reached the main Baños highway near Las Juntas bridge, according to eye-witnesses and live radio reports. PDC-2 occurred shortly thereafter (00H24) and its deposits lie directly upon those of PDC-1. Ash cloud surges (ACS) were associated with both PDC-1 and 2, although those of PDC-1 dominate and cover a greater area on the cone's W and SW flanks. PDC-3 is not a single flow event, but refers to a series of granular pyroclastic flows that occurred after the cessation of ash-forming activity (after 01H14), that had a restricted distribution directly down slope from the crater's lowest rim, and that developed a notable channel and levee morphology. These three PDC events were monitored by seismic, infrasound, and AFM instruments, but were only occasionally visible due to nightfall and cloudy, ashy conditions. The PDC-3 series generated only background noise, without discrete seismic or acoustic outburst events.

3.2. PDC-1 and 2 – distribution

The cone's upper flanks have a nearly constant slope gradient of 28° , while its intermediate flanks have gradients that average 16 – 19° and the lowest flanks have variable gradients of ~ 13 – 14° . The PDC flows descended the steep NW, W, and SW flanks and then became increasingly channeled into the many gullies that drain the intermediate slopes. PDC-1 and 2 descended most gullies of the cone's northern and western sides, from the Quebradas (=ravine) Vascún and Pucuyacu in the N, to Q. Juive Grande, Cusúa, and Achupashal in the NW, to



Fig. 7. Upstream view of the Chambo river valley dammed by a series of PDC flows and fans with the resulting lake behind. Note the steam from rootless fumaroles in valley fill above the letters “CHONTA”. Chambo lake drained in 18 August. Arrows show PDC flow directions.

Q. Chontapamba, Rea, and Confesionario on the W and SW, and to Q. Mapayacu on the SSW side (see Fig. 2). These gullies are typically 10–30 m wide, 10–15 m deep, have steep interior walls, and descend radially from the cone. In all cases the flows that reached the surrounding valleys of the Puela, Chambo, and Pastaza rivers had traveled 7.5 to 8.6 km. Only traces of flow deposits remain in the ravines with high to medium gradients. The flows incorporated loose material (older lavas and tephra, trees and branches) that was encountered en route and which was then deposited along with the PDC debris in local areas of aggradation, on the fans, or at the valley bottoms.

Upon reaching the floors of these valleys, PDC-1 and 2 and the accompanying ACS filled the valleys with hot pyroclastic material. The Chambo river was dammed from Q. Cusúa to Q. Achupashal and from Q. Chontapamba to Q. Rea, forming a series of coalescing dams that held until 18 August. As the river rose and invaded the hot material, rootless fumaroles were generated (Fig. 7). It should be noted that the PDC-2 deposits are poorly represented on the SW flanks, due either to its smaller volume or its being covered by remobilized ash.

On the NNE flanks PDC descended the Vascún and Pucayacu valleys for 7 and 4 km, respectively, but were relatively small in volume and did not reach the foot of the volcano. The PDC in Q. Confesionario stopped only ~150 m short of reaching the Chambo river. The adjacent Choglontus arroyo lost its pyroclastic flow, when the flow overrode its left bank on a curve and entered Q. Mapayacu where it took a more southerly course and reached the Puela river and Palitagua village (Fig. 2), which resulted in the deaths of six inhabitants who hadn't heeded the evacuation orders. The PDC deposits dammed this river for a few days and upon failure produced a large lahar.

Evidence that PDC had descended the E, SE, and S sides of the edifice is lacking, despite aerial searches. Apparently fountain collapses and only low column collapses generated the PDC, as the PDC were restricted to the cone's western flanks. The difference in elevation between the crater and access to the eastern flank is ~250 vertical meters, implying that the fountain collapses were of low altitude and centered over the crater or inclined slightly to the W. The winds that night were directed to the west as usual, and were not especially forceful, consequently it is not likely that they played a significant role in orienting the clast-rich column collapses.

3.3. PDC-1 and 2 – description of their deposits

The PDC-1 and 2 deposits share many of the same characteristics and will be discussed together. The PDC-1 deposit is a rosy-brown, poorly-sorted volcanic breccia that is overlain by a 0.1–2.0 m thick layer of well-sorted sandy ash, considered to be its ACS unit. The PDC-2 breccia deposits are similar to those of PDC-1 in grain-size and components, but are blackish-brown in color due to the presence of more black juvenile material and have an incipient lobe morphology. These two principal PDC were readily recognized based upon their morphology, color, and their stratigraphic relations. They overlie deposits of the 15 July 2006 eruption at the middle elevations and older lahar deposits in the lower JG valley. They are best exposed on the JG and the adjacent La Pampa fans, where they spread out laterally and are not totally buried by younger lahars. Around the NW and W flanks of the volcano, both PDC-1 and 2 deposits are 1–5 m-thick. The PDC-1 deposits are also found as thin overbank layers along the 10–20 m deep gullies or rarely in the bottom of the gullies themselves, implying that the flows were sufficiently fluidized to leave their channels. The associated ACS typically spread out across the interflaves.

At the distal end of the JG fan the PDC-1 deposits are low-aspect-ratio, planar deposits, ~1 m thick and tens of meters wide (Fig. 8A, B). PDC-2 deposits however form poorly developed lobes with slightly convex cross-sections and frontal and lateral limits that are up to 30 cm high (Fig. 8D). Both PDC-1 and 2 are massive, non-stratified, poorly-sorted, matrix-supported deposits. The surface of the distal PDC-1 unit is littered with unburnt broken branches and a thin fine-ash layer, a remnant of its accompanying ACS; neither the branches nor the ash layer is found on nearby PDC-2 units (Fig. 8A, B), indicating that the principal ACS accompanied the PDC-1 flow.

Being the first large flow, PDC-1 was able to incorporate a notable quantity of loose pre-existing rocks and fine material in its steep descent down the cone's upper and intermediate flanks. Furthermore it apparently entrained significant quantities of air in its descent over irregular topography that helped to fluidize the flow, resulting in normal-graded breccia deposits at the foot of the intermediate slopes (Fig. 10A). However, toward the distal ends of these same flows their deposits locally show incipient reverse gradation (Fig. 8C),



Fig. 8. (A) At Juive Grande the widespread planar PDC-1 deposit is blanketed with tan-colored ash and unburnt branches from its ACS. It is overridden by the black clast-rich PDC-2 deposit with its semi-lobe morphology; it lacks an ACS ash at this distal end. Combined thickness of both PDC is ~3 m. (B) Near Cusúa PDC-1 arrived as a more fluidized wave, with a greater matrix content and its ACS blanket. PDC-2 was also more fluidized in this sector and without an ACS cover. (C) The PDC sequence on the lower Juive Grande fan. Note that PDC-1 and 2 deposits are slightly reverse-graded, while that of distal PDC-3 is clearly granular and normally graded. PDC-1 deposits tend to be redder in color and carry accidental clasts. PDC-2 and 3 deposits tend to be blacker and locally crudely stratified. (D) On the lower JG plain PDC-2 lobes overlie the PDC-1 deposits. Note the lobe morphology and its abundant but small molten clots and the few accidental lithic clasts. Red scrapper is a 30 cm-long scale.

presumably due to a certain loss of fluidization. As discussed later, these flows were fast (~21 m/s) and forceful.

3.4. PDC-1 and 2 – components and granulometry

An examination of the fine-grained (≤ 2 mm) portion of these PDC deposits by binocular microscope indicated that they typically consist of black to brown scoria fragments (5–15%), black angular lithic clasts (5–15%), free crystals (2–3%), and the remaining 67–88% of volcanic glass. Within the glass one can discern ~10% lath-shaped plagioclase (0.7–1.0 mm in size) and 3–5% crystals (≤ 1 mm) of clinopyroxene (cpx), orthopyroxene (opx), olivine, and opaque iron oxides. The glass particles fall in the size range of 0.05 to 2.0 mm, being relatively uniform in their size distribution, an aspect frequently observed in vulcanian-generated deposits and often attributed to high energy fragmentation (Cashman et al., 2000).

Two types of glass dominate the matrix. The first is a light to dark green, transparent glass that generally has a low percentage of vesicles (5–10%; maximum of 30% in a few grains), or no vesicles. These are generally small (0.01–0.03 mm in diameter; a few are 0.08–0.09 mm) and most commonly spherical in shape. The second glass type is slightly tan to gray in color, which is possibly due to a large population of very small bubbles and/or to very small microlites (≤ 0.005 mm). This glass type also has vesicles similar in size and shape to those of the green glass. In both glass types elongate bubbles are occasionally seen and more rarely tube-shaped vesicles. Given that these glass types don't carry significant numbers of crystals or vesicles, it would seem that the magma was not especially viscous, also suggested by the occasional presence of grains of spindle-shaped glass and Pele's hair. After studying the glassy matrix Hanson et al. (2009) concluded that two batches of

magma were involved, one microlite-rich and the other not, which likely affected the magma's viscosity and other rheological properties.

Both PDC-1 and 2 deposits gave similar granulometric analyses with sorting coefficients typical of many granular pyroclastic flows (Fig. 9). Note that clasts ≥ 5 cm are not included in the granulometric analyses and in some cases these may amount to 25–50 vol.% of the deposit. The total volume of the very fine-grained material is sub-estimated as it was presumably winnowed out to form the ACS units. Compared to PDC-2, the PDC-1 deposits generally have more variable contents of both the sand-size fraction (0.06–2 mm) (35–95%) and the gravel-size fraction (2–64 mm) (5–65%). A larger percentage ($\leq 40\%$) of gravel and cobble-size (64–256 mm) fragments characterize the basal layers of the central flow path upon the JG fan (Fig. 10A), as well as at the distal ends of both pyroclastic flows. PDC-1 units have varied sorting coefficients, probably due to the greater size range of the entrained accidental clasts picked up during descent, whose volume is estimated at 1–10% of the total. On the other hand PDC-2 deposits have more restricted size fractions; for example, the sand-size fraction is ~60–80% and the gravel-size fraction around 20–40%. PDC-2 has relatively constant sorting coefficients (note its tight curves) implying that most components came from the eruption itself and that little accidental material was entrained en route.

The deposits of both PDC-1 and 2 are $\geq 50\%$ rich in sand-size grains (matrix) but also carry significant amounts of gravel and cobble-size clasts that are more common and larger in the basal layers (Fig. 10A). The clasts consist of dense angular fragments of both gray and black juvenile andesites, as well as reddish oxidized fragments of lava. The most characteristic fragments are the remnants of the so-called molten clots, broken and abraded during their eruption and descent, and now form a major part of the coarse fraction of the PDC-1 and 2 deposits. The term

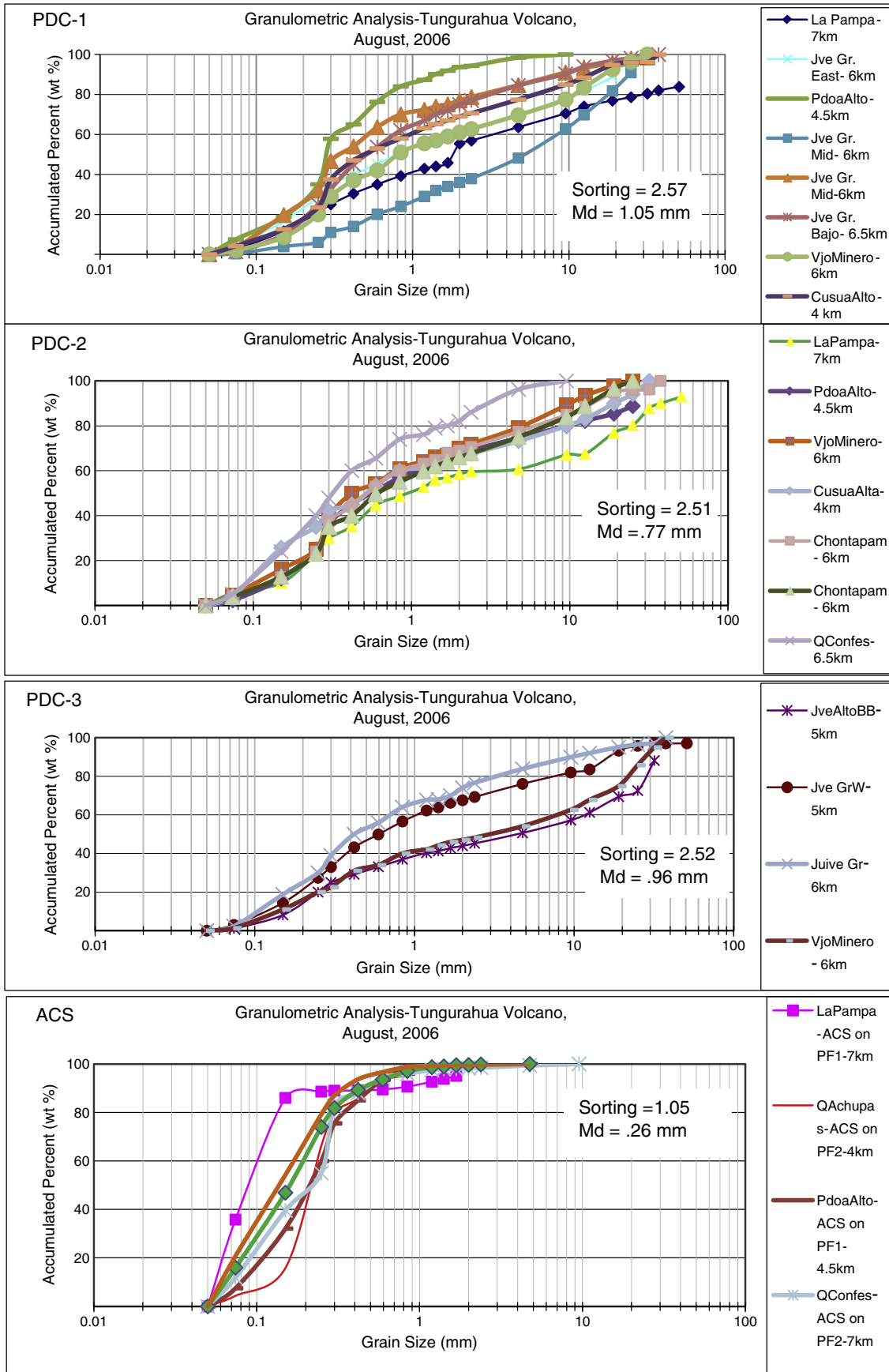


Fig. 9. Granulometric analyses of the three major PDC and the main ACS deposits. Clasts larger than 5 cm are not included. If they were included, the PDC curves would be flatter and would further confirm the very poor sorting of the PDC deposits.

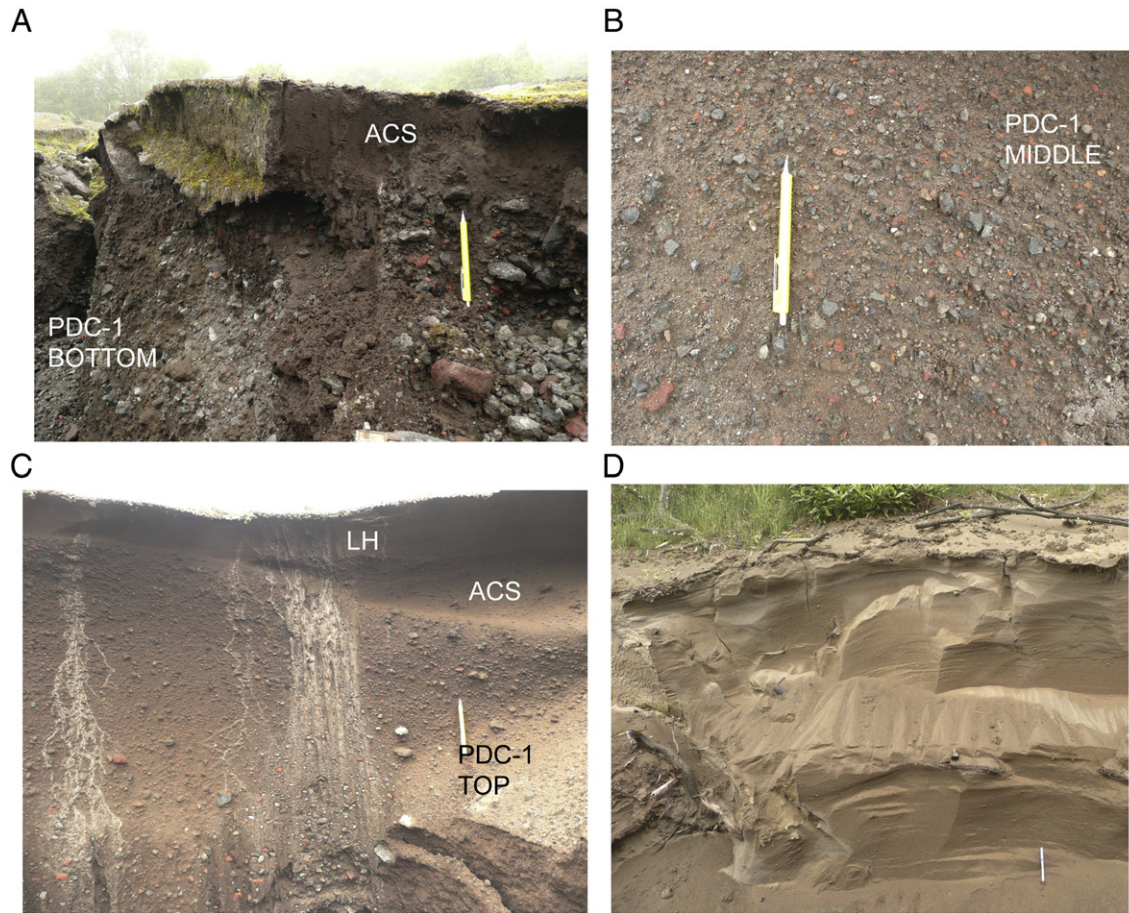


Fig. 10. A, B, C, and D demonstrate that the PDC-1 is a normally graded deposit, with a high percentage of vitric-rich fines, typical of the central JG depositional fan. (A) The clast-rich basal portion of the PDC-1 deposit with its overlying ACS layer. Note its polilithic nature comprised of many clasts picked up en route from the summit. (B) Typical appearance of the middle portion of many PDC-1 deposits consisting of gravel-sized clasts in an abundant sand-size ashy matrix. Note the angular gray, black, and red clasts of both juvenile and accidental origin. (C) The upper portions of most PDC-1 deposits are matrix-rich with a subordinate fraction of gravel-sized clasts that become smaller upward. Note the overlying ACS unit and a later lahar bed on top. (D) Weakly-stratified, very fine grained ACS deposits adorning the sides of JG valley. The flow was from right to left. At bottom left are partially carbonized branches buried within the deposit. Scorching branches lie on its surface. Pencil for scale.

'molten clot' refers to the dark gray to black cauliflower-shaped lava clasts whose entire perimeter has a molten appearance (Fig. 11A, C). These are unlike breadcrumb textures of bombs that generally have obvious expansion fractures and are characteristic of more viscous, siliceous magmas (Alvarado and Soto, 2002; Wright et al., 2007). The molten clots have uniformly thick glassy rinds that envelope the clot's entire 360° perimeter and have no or only incipient expansion cracks. They have a homogeneous interior with small vesicles that are often arranged in concentric patterns, implying that the entire clot had expanded uniformly in radial fashion. This and their quenched exterior indicate that they cooled quickly in a free medium, such as in air or a gas. As such, they are thought to have formed by the violent ejection of molten blobs of magma into the air during explosive events, an interpretation also suggested by Miyabuchi et al. (2006). Similar molten clots characterize PDC of lobe and channel morphology at Mt. Spurr (Miller et al., 1995), however these became deformed in transit, suggesting that they were hotter than those reported here. Conversely, similar clots observed at Arenal volcano (Alvarado and Soto, 2002; Cole et al., 2005) were formed when lava spilled out of the crater's lava lake; these were hot and plastic-enough to also deform in transit, giving them a crude pancake-like appearance. Pristine clots are common in PDC-3 deposits and most are neither deformed nor fractured.

Five principal types of components characterize the gravel-size fraction of the PDC-1 and 2 deposits. Non-juvenile accidental components picked up on the upper flanks of the cone are significant in PDC-1 deposits and include (a) bright red, slightly vesicular scoria, (b) light

gray, aphanitic to slightly porphyritic, non-vesicular andesite, and (c) dark gray to black, glassy to aphanitic, non-vesicular andesitic lava fragments whose crystal content differs from that of the juvenile magma. Dark gray to black juvenile andesitic fragments are the most abundant constituent of both PDC-1 and 2, amounting to ~60–80% of the gravel fraction. Olive-green-colored, frothy vesicular, light-weight scoria also occurs but mainly in the Cusúa to Chontapamba areas, WNW of the crater; it is more abundant in the PDC-2 beds (15–50%) than in the PDC-1 deposits (~20%) on the Cusúa fan.

3.5. Ash cloud surge deposits

Ash cloud surges (ACS) accompanied both PDC-1 and 2 flows. The ACS-1 deposit directly overlies its PDC-1 layer and has the greater volume and distribution of any ACS deposit. The ACS beds have gradational contacts with their underlying PDC, implying that they were a continuum (Fig. 10C); they in turn are clearly overlain by the later PDC-3 deposits. Basal surges that might underlie the PDC were not observed. The deposits of both ACS are rosy-brown in color, generally well-sorted, and are comprised mainly of fine sand-sized grains, but at times they carry $\leq 2\%$ gravel and pebble-sized clasts. The deposits are internally homogeneous and vary from 1–2 cm to 10–15 cm in thickness, although some leeside accumulations are more than 2 m thick (Fig. 10D). Occasionally they show subtle stratification and cross-bedding. Granulometric analyses of several ACS deposits clearly show their well-sorted character and that their grain size is generally less

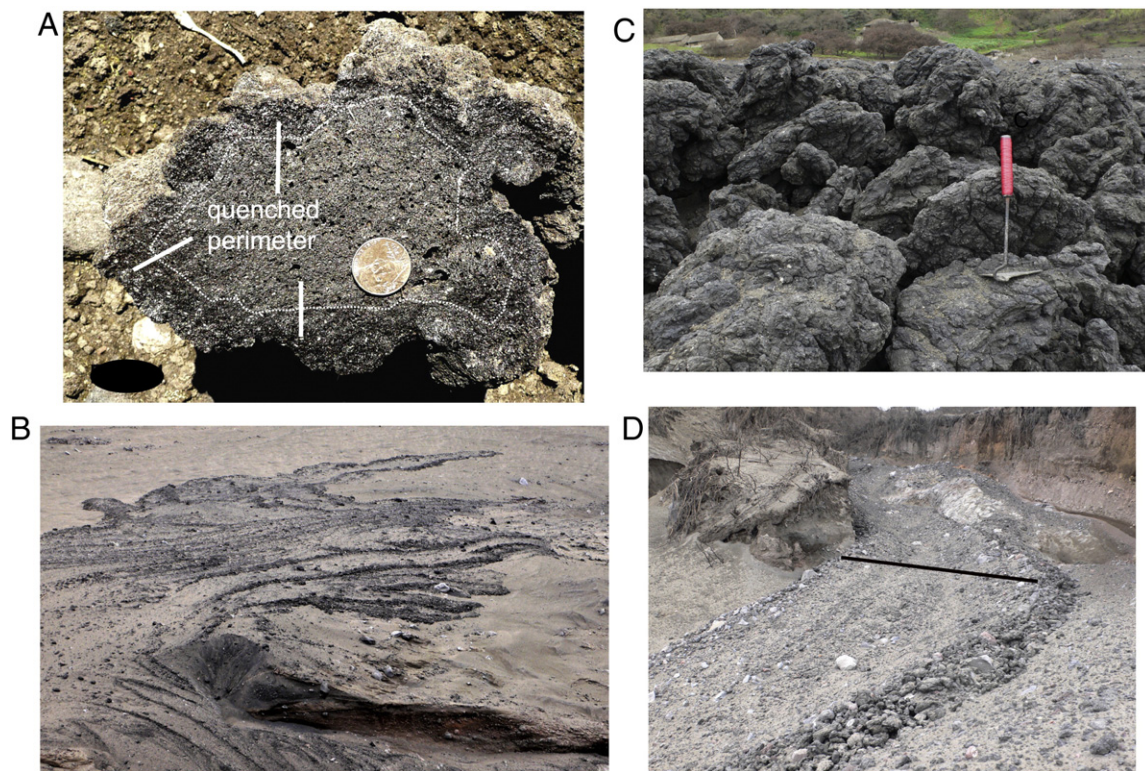


Fig. 11. (A) Typical molten clast displaying a uniformly thick, quenched glassy rind around the entire perimeter of the clast, implying that it was cooled quickly by aerial transport. In other samples small vesicles are arranged in a concentric pattern, again suggesting that the clots expanded radially without interference. (B) A series of PDC-3 lobes that terminated at the foot of the steep cone and upon an intermediate terrace of the JG fan. Note the lobe morphology, well-defined levees, and empty channels. The longer empty channel that crosses the series is about 10 m wide. Super-elevation modeling of the three flows that terminate after ascending the small hill in the center of the photo suggests that they had velocities of about 4 m/s. (C) Typical solidified molten clots up to 50 cm in size rafted up onto flow levees. Note that the so-called molten texture occurs on all sides of the blocks, presumably due to quenching in flight, and not to a lava lake spillout. (D) A late PDC-3 flow with well-defined asymmetric levees and an empty channel, 8 m wide (bar). Flow overlies an earlier, more fluidized PDC. Super-elevation modeling on this curve suggests that the flow had a velocity of 3.5 to 4 m/s. Intermediate JG fan.

than 0.3 mm (Fig. 9). In their study of the air-fall tephra from this eruption, Eychenne et al. (2012) found a bimodal grain-size distribution in which plume-derived ash was coarser than 0.25 mm, while ACS-derived elutriated ash was much finer. The ACS deposits carry a high percentage of the same two types of glass components observed in the PDC-1 and 2 deposits and only a trace of the denser particles (crystals and lithics).

The ACS deposits are found as channel, overbank, and floodplain deposits along all quebradas in which PDC-1 and 2 traveled, from JG in the north to Mapayacu valley in the south. The larger deposits cover the interfluvies between neighboring ravines and have centrimetric thicknesses. On the upper JG fan, surges climbed 10 m up the northern wall of the canyon, turned, and then descended back onto the JG fan, leaving withered, but unburnt cane stalks as guides to the path that the ACS had followed. In the deep narrow ravines of the lower west flanks, the ACS often spilled out of their channels and swept across the adjacent floodplains for 50–100 m, especially in the Cusúa to Rea areas. Surges with significant volumes descended the Cusúa, Achupashal, and Pirámide ravines and crossed the Chambo river, where they ascended the valley's opposite side for 50 m and impacted a hamlet near Cotaló (Fig. 2). Furthermore, thick ACS deposits, in addition to their PDC-1 and 2's deposits, contributed to the damming of the Chambo river. ACS of lesser temperature descended other arroyos of the lower W flank without burning or drying out the vegetation, their cooler temperatures apparently due to their smaller volume and the greater distance traveled.

Due to the steep flanks of the cone, the PDC presumably entrained and heated air which led to extensive elutriation and a widespread ACS distribution. On channel floodplains not overrun by the PDC, such as at IG's Cusúa Station (Fig. 2), the ACS had sufficient velocity to rip

out solar panels, antennas, and their supports. There, the surge melted most exterior plastic components, abraded the 1/2 cm-thick bark of trees to heights of 5–6 m, and lightly scorched its exposed wood core. Farther from the ravine the ACS were only able to strip the standing trees of their branches and leaves. In other areas the brush and leaves were left intact, but the accompanying heat killed the vegetation, as well as livestock tethered in interfluvie pastures. On two occasions where ravines made abrupt turns, ACS decoupled from their PDC and continued along their preceding paths, traveling hundreds of meters farther down slope, while the PDC remained in the channel. Such was the case in both the Achupashal and Mapayacu channels, where ACS left their channels and covered more than one hundred thousand square meters with dune deposits (Douillet et al., 2010).

3.6. PDC-3 – distribution

The most spectacular deposits of the three pyroclastic flow events are those of PDC-3. These are readily recognized by their many flow lobes that clearly rest upon the earlier PDC-1 and 2 deposits and their respective ACS layers. The PDC-3 deposits are blackish-gray in color, have prominent channel and levee morphology, and a notable abundance of large dark gray to black molten clots (Fig. 11B, C).

PDC-3 deposits are observed only in the Mandur, Hacienda, and Cusúa ravines and in the three main arroyos of the JG drainage (Fig. 2). All of these drainages head on the low NW rim of the crater, which explains the limited distribution of PDC-3 units on this side of the cone. The flows were restricted to the bottom of these ravines, where their confinement to narrow channels greatly reduced the possibility of air entrainment and consequently their fluidity, without which they could not form planar deposits. Thus, they formed narrow lobes



Fig. 12. Blocky lava flow of Phase IV in Q, Achupashal. Blocks and slabs of scoriaceous andesite form a carapace overlying a core of massive lava. Lava issued from the crater less than 20 h after the explosive activity ended (01H14–17 Aug.).

that were often kilometers long. PDC-3 was not accompanied by surge flows, as neither basal surge nor ACS deposits were observed associated with the PDC-3 lobes on the morning after the eruption. Apparently PDC-3's slow velocities and limited air entrainment precluded elutriation of fine ash particles.

3.7. PDC-3 – lobe morphology and formation

The PDC-3 deposits demonstrate well-developed lobe and channel morphology, the lobes being typically 5 to 10 m wide, with parallel levees and empty channels (Fig. 11B, D). The first PDC-3 flows reached the foot of the JG fan about 7 km distant, but subsequent flows were progressively shorter, the last flows descending only to the foot of the steep cone, a distance of 3 km.

The morphologically pristine PDC-3 lobes have termini or snouts, up to 2 m in height that are notably convex in cross-section and without levees. Upstream the lobes are bounded by well-developed parallel levees up to 1–1.5 m high that enclose empty flow channels. The lobes are mainly comprised of large abundant molten clots that average 0.2–1 m in diameter, sub-angular lithic clasts, and a predominantly sandy matrix. Curiously, accumulations of molten clasts and lithic debris are occasionally found abandoned within empty flow channels; apparently these are the remnants of pulses of flow material whose momentum was insufficient to carry them farther down the channel. Such accumulations were occasionally found repeated in the same lobe channel, indicating that the channel had been reused by a series of sequential pulses, each carrying a progressively decreased supply of clasts and lava debris. Individual lobes had volumes estimated at 1500 to 5000 m³.

Because the PDC-3 flows descended channels that had already been scoured by preceding PDC events, they had little impact upon the already devastated vegetation. No carbonized wood was found in these deposits, and nearby vegetation was unaffected by heat.

PDC-3's velocities were estimated by employing super-elevation calculations on two late flows that occur at the top of the depositional fan, where their geometric situation favored such an estimate (Pierson,

1985). A flow's run-up over a small hill on the JG fan and its subsequent halt (Fig. 11B) suggests a maximum velocity of 4.4–5.5 m/s. Nearby, a flow's super-elevation path on a tight bend in a channel (Fig. 11D) gave a velocity of 3.5–3.7 m/s. These PDC-3 flows were much slower than that of PDC-1 (~21 m/s) or those of the previous evening (~30 m/s). At Mt. Spurr pyroclastic flows similar in composition and lobe morphology to that of Tungurahua also had slow velocities (~6 m/s) and apparently were not fluidized (Miller et al., 1995).

The earliest PDC-3 flows traveled farther, were more voluminous, and likely had greater velocities, although this could not be verified. The last flows however only reached the upper end of the JG fan and were slow, as suggested by these velocity estimates.

3.8. PDC-3 – components and granulometry

Granulometric analyses of the PDC-3 units have sorting coefficients similar to those of PDC-1 and 2 (Fig. 9). However, these PDC-3 values would be far larger, implying very poor sorting, if their large molten clots were included in the analysis. The lobes are clast-rich on their outer surfaces, but internal portions have a significant fine-grained matrix (40–70%). The matrix has a yellowish-brown color and is composed of friable, coarse silt-size to fine sand-size juvenile grains (94%) and accidental lithic material (6%). The matrices carry the same components as those observed in PDC-1 and 2. In contrast, the coarser fraction (≥ 2 mm) makes up 30–60% of the flow deposit and is dominated by molten clots and their fragments (80%). Denser non-juvenile fragments make up to 5–10% of the flow's volume and are more common in the interior of the deposit, where there are relatively fewer molten clasts. The PDC-3 deposits carry more and larger juvenile clasts than those of the earlier PDC.

The fact that most molten clots of PDC-3 are not extensively abraded or fractured suggests that they had not suffered hard impacts during transport. This might be the case if these clots were cushioned in the fine-grained matrix, if their lesser densities allowed them to segregate upwards, and if transport was relatively slow.

3.9. PDC-3 – origin

PDC-3's origin is assigned to the post-eruptive period (after 01H14 of 17 Aug.) as no ash was found mantling its deposits. This conclusion is corroborated by the fact that the PDC-3 deposits carry large unbroken molten clots that would not likely have survived the late explosive activity. More probably the clots formed by low-level lava fountaining or by spilling out of a lava lake in the waning stages of the eruption. The uniformity in shape and size of the lobe channels, on both the upper and lower depositional fans, leaves the impression that the lobes were the result of a relatively slow but constant supply of molten clots and lithic debris, generated by a continuous spilling of magma from the crater. This stream of eruptive debris likely descended in conveyor-belt fashion down the slopes immediately below the crater and later divided into several lobes upon reaching the upper depositional fan (Fig. 11B). Given that the molten clots arrived onto the cone's intermediate slopes in pristine condition argue that they rode or floated down the lobe channels on a cushion of cascading debris.

4. Associated ash-fall deposits

Scoria lapilli (2–3 cm in diameter) began to fall in large quantities beginning at 00H44 (17 Aug.), especially toward the NW, as well as in the Cusúa and Cotaló–Paillate areas to the W, and in the greater Puela–Choglontus area to the SW of the cone. Ash fell over a 40–50 km radius in a westerly direction (Troncoso et al., 2006; Eychenne et al., 2012). In 18 August fine ash arrived in Cuenca (05H55) and in Guayaquil (14H20), located 180 km to the S and SW, respectively.

Observers on the cone's W and SW flanks reported white pumice falling with the brown scoria at the end of the eruption. The next day we confirmed the presence of scarce, highly-vesiculated, off-white, lightweight pumice on the surficial deposits, clearly emitted late in the eruption. In sharp contrast to the homogeneous andesites (58–59 wt.% SiO₂) erupted since 1999, this pumice had 61–65 wt.% SiO₂ (Samaniego et al., 2011). These authors suggest that these more silicic melts may be remnants of the 1886 magma and that during the paroxysmal phase of the eruption they were remobilized and accompanied the final andesitic eruptions. If so, their inclusion in the magma might have contributed to the increased explosivity of the midnight events.

5. Flow velocity, dynamic force, and heat impact of the PDC

PDC velocities during phases I and II were based on the travel times, calculated using the time difference between the seismic signals of discrete outbursts and PDC arrival times at monitoring stations. Discrete events at 21H13, 21H43, and 22H15 (16 Aug.) were well-registered at the Cusúa BB station (see Fig. 3A, B), each of which was followed minutes later by a strong tremor signal (10–21 Hz) that lasted about 5–6 min, which we interpreted as the passage of a PDC. Taking the largest amplitude signals of these tremors to represent the PDC closest approach to the Cusúa station, we obtain velocities of 32.4, 30.7, and 33 m/s for these three PDC events, respectively. These rapid, well-constrained velocities correspond to an uninterrupted slope distance of 4.95 km and a vertical drop of 2020 m. The fact that the seismic signals of all three explosion-tremor episodes are very similar in shape and timing strongly implies that they are PDC of similar origin and travel paths. Each of these flow events was corroborated by visual confirmation of an incandescent flow and registered in the logbook. In addition the 21H43 flow was also sighted descending the upper JG valley and its passage close to the Juive AFM station was recorded; its slower velocity of 14.6 m/s is attributed to its more sinuous path and stepped terraces. Unfortunately in Phase III accurate PDC velocities could not be calculated due to the chaotic nature of the seismic signals.

The dynamic impact of the PDC can be summarized as follows. In terms of man-made structures, the PDC had the force to carry away

items of appreciable surface area, such as solar panels and rain gauge, as well as bend and completely deform metal pipes used for masts. Five meter high three-legged metal towers and concrete instrument closets were unaffected. Importantly, all BB stations which were housed in thick plastic, coffin-size trunks, and buried under ≥ 30 cm of soil were unaffected by the PDC and continued to operate, although they had lost their above ground telemetry, solar panels, antennas, and infrasound sensors.

The vegetation suffered complete destruction in the arroyos transited by PDC. The adjacent banks of the arroyos were razed by the more dilute, upper parts of the PDC that carried gravel-sized clasts in a fine sand-size matrix-rich flow. There, the flows bent and felled trees, abraded and stripped trees of their bark, but rarely scorched the interior wood. Trees up to 20 cm in diameter were knocked down in high velocity paths, the majority being aligned with the likely flow path. At distances out to 50 m from the arroyo, the few trees that remained standing had their bark stripped on their windward side. Brush and low vegetation were buried by 10–20 cm of surge ash. At distances of 30–100 m from the arroyo the impact became more variable. Devastated areas alternate with groups of trees that remained standing but that had lost their branches and leaves. In the lower reaches of some ravines where PDC deposits are not present, the brush was flattened and killed by heat from a passing ACS. There, tree bark was not abraded, only lightly scorched by an ACS.

Wood ignition temperatures by radiant heat have been studied in some detail (Babrauskas, 2001) and depend upon the characteristics of the wood (density, moisture content, thermal conductivity), as well as the orientation of the log and the heat flux rate. Notably, in most cases scorching (“glowing ignition”) was minimum, only slightly affecting the solid wood of the abraded trunks of standing trees, with no evidence of deep charcoal formation. Nor was there any evidence that these scorched trees had caught fire. Babrauskas (2001) reports that the minimum glowing ignition temperatures would be ~ 250 °C and that a few minutes duration would be sufficient to attain this state. At higher heat flux rates, as in the temperature range between glowing ignition and flame ignition, the temperatures would vary between 255° and 300 °C. He concludes that temperatures under 300 °C generally lead to charring, while over 300 °C increased gas release promotes flame ignition. At Juive Grande wooden structures such as shacks and fences did not catch fire. As such, the PDC discussed here (the dilute upper part of the PDC and the accompanying ACS) probably remained below this 250°–300 °C range.

Nevertheless, branches and tree trunks buried in the PDC and surge deposits at depths of ≥ 50 –100 cm were everywhere well-carbonized. A wood telephone pole, 20 cm in diameter, was thoroughly carbonized below ground level in a 2 m thick PDC-1 deposit, a process that occurred in less than 8 h; the pole's above-surface extent was not noticeably affected. According to Café (2007), wood becomes charcoal at $T \geq 120^\circ$ –150 °C at the rate of 30–50 mm/h.

At the lower end of the JG fan, additional evidence of heat effects was found. Marginal to a PDC flow large pigs were mortally affected by the heat wave. Elsewhere, cattle apparently died by inhaling hot gases and had no visible exterior affectation. Within an unfinished concrete house without windows or doors, but adjacent to a PDC lobe, glass, metal, and rubber items were clearly unaffected by the heat, as were a thick plastic water barrel and a polyethylene rope. Thin plastic curtains and a squeezable plastic cup, however, were deformed but not melted, again suggesting low temperatures. Outside the house plastic electrical switch covers and a plastic hose had melted. Café (2007) reports that most thin plastic items melt between 100 °C and 250 °C. In conclusion the limited evidence suggests that the temperatures of the PDC at the lower reaches of their paths ranged from ~ 100 °C to ≤ 300 °C. Comparable low temperatures (180–220 °C) were reported for some PDC deposits at Montserrat (Cole et al., 2002).

In summary, although thermal images of Tungurahua's crater vent taken in over-flights gave minimum temperatures of ≥ 700 °C

(P. Ramón, pers. comm.), air temperatures were only several hundred degrees centigrade at the distal end of the PDC.

6. Discussion

The 16–17 August 2006 eruption cycle of Tungurahua was well monitored, both instrumentally and chronologically. Initially the eruptive style was dominated by progressively stronger strombolian activity that lasted hours interspersed with discrete high energy outbursts generally interpreted as vulcanian explosions. Small PDC often accompanied these eruptive bursts. Activity climaxed at midnight in subplinian style, highlighted by intense fire fountaining, continuous jetting, and occasional strong outbursts. This unrelenting period of activity produced a high eruption column and a series of large PDC, including PDC-1 and 2. Strong seismic and acoustic energies from discrete eruptive outbursts were recorded throughout the eruption cycle and displayed SRD and IRP values that were often much greater than those registered for vulcanian explosions at other volcanoes.

Seismic energy of the strongest events reached a maximum of $4.04 \text{ E} + 10 \text{ J}$. with an averaged SRD of 855 cm^2 . This is far greater than explosions of vulcanian eruptive events at Augustine Volcano, Alaska that had maximum values of 178 cm^2 (McNutt et al., 2010; Vallance et al., 2010). In fact, almost all discrete outburst events recorded at Tungurahua during this eruptive cycle displayed seismic amplitudes far greater than those recorded at Augustine. In total, seismic energy release calculated for the entire hour of Tungurahua's midnight eruptions reached an incredible $3.4 \text{ E} + 11 \text{ J}$.

Petersen et al. (2006) reported acoustic energy values for Augustine volcano ranging from 5.8 to $27 \text{ E} + 08 \text{ J}$, for high-amplitude impulsive eruptive events bearing N-shaped waveforms. Discrete outbursts recorded at Tungurahua did not display similar acoustic waveform characteristics in 16–17 August, likely due to interference from other volcanic signals. Nevertheless infrasound energy values from many of the discrete impulsive events (interpreted as vulcanian explosions) were larger than those recorded at Augustine volcano, such as activity during Phase II between 22H15 (16 Aug.) and 00H02 (17 Aug.). During Phase III, visual and seismo-acoustic identification of the strongest outbursts (high energy spikes), such as those at 00H49 and 01H06, attained acoustic energies almost an order of magnitude larger than the explosions at Augustine. These infrasound energies are also two orders of magnitude greater than those reported for explosions at Fuego volcano, Guatemala (Marchetti et al., 2009).

Most PDC originated with intense fire fountaining and/or by strong impulsive bursts of activity and their passage was confirmed visually and/or was recorded by a monitoring station. Other PDC whose passage was detected by instruments, but whose origin could not be related to discrete eruptive outbursts, were attributed to the sluffing off of accumulated ejecta from the crater rim. In contrast an origin attributed to the boiling over of a crater lake or spatter from the top of the magma conduit would not be in agreement with the high energy regime at the crater during strong strombolian or subplinian activity.

The largest pyroclastic flows, PDC-1 and 2, are associated with the paroxysmal period between 00H20 and 00H24 of 17 August. These were restricted to the western half of the volcano and they did not descend the east or southeast sides of the cone, implying that if column collapses occurred, they were no higher than several hundred meters above the crater. Low column collapses were referred to as “fountain collapses” at Montserrat (Druitt et al., 2002), which were well-documented photographically. There, large volumes of material were expelled, which then fell back or collapsed onto the upper slopes of the vent, initiating PDC. A similar origin is envisioned for Tungurahua's larger pyroclastic flows.

The most notable feature of the PDC was the variability in the fluidity of the early flows as compared to the last flows. Upon the depositional fan, the PDC-1 and 2 flows spread out laterally leaving normal-graded, thin planar units, implying they had been somewhat fluidized, attributed here to greater air entrainment during their long steep descents.

Contrarily, the late PDC-3 flows – the product of low level lava fountaining or by spill outs from the crater – descended from the crater's lowest rim (NW side) and traveled down slope as slow conveyor belt streams that formed narrow lobes which closely followed the bottom of the descending ravines, thus limiting air entrainment and consequently their fluidity. The PDC-3 flows were granular flows that developed good lobe and channel morphology. These were followed a few hours later by the emission of blocky lava flows of the same, but greatly degassed andesite.

A total volume of the PDC deposits is estimated to be about $38.7 \times 10^6 \text{ m}^3$, the sum of $17.3 \times 10^6 \text{ m}^3$ (PDC-1), $8.5 \times 10^6 \text{ m}^3$ (PDC-2), $1.02 \times 10^6 \text{ m}^3$ (PDC-3), and $11.9 \times 10^6 \text{ m}^3$ (ACS). Of this total volume, $30.5 \times 10^6 \text{ m}^3$ is attributed to the juvenile contribution during the 16–17 August eruption, whose DRE equivalent is about $18.7 \times 10^6 \text{ m}^3$. Eychenne et al. (2012) assign a total bulk tephra volume of $42\text{--}57 \times 10^6 \text{ m}^3$. The late lava flow had a volume estimated at $\sim 7 \times 10^6 \text{ m}^3$ (J. Bustillos, pers. com. 2012) (Fig. 12). As such the 16–17 August eruption had a total output of $\sim 0.1 \text{ km}^3$.

Some have described the paroxysmal phase of the 16–17 August eruption of Tungurahua as plinian in nature (Fee et al., 2010; Steffke et al., 2010), based primarily upon its plume height ($\sim 22.5 \text{ km}$), however we judge the overall eruptive character of this phase to be subplinian with occasional discrete high energy outbursts. This we base upon a) the continuous high energy emission rate that lasted 34 min, b) the relatively small volume (0.1 km^3) of volcanic ejecta, c) the overall character of the eruptive cycle is more akin to its intermediate chemical composition, and d) its maximum plume height of $\sim 22.5 \text{ km}$ is similar to heights reported for subplinian events (Cioni et al., 2000).

Acknowledgment

The authors would like to acknowledge the momentous efforts of the entire IG staff, especially the electronic and scientific personnel, for the successful monitoring of Tungurahua volcano and the continued evaluation and interpretation of the endless data stream. Without the selfless help of the Chavez Family of Baños, the IG would not have an observatory site. The sophisticated level of monitoring and data interpretation is due to the help received from Japan International Cooperation Agency, the United States Geological Survey, the Escuela Politécnica Nacional, the Ecuadorian government, and the Institut de Recherche pour le Développement. In addition the authors thank Pablo Samaniego for reviewing an early manuscript and the two anonymous reviewers of the submitted draft.

References

- Alvarado, G.E., Soto, G.J., 2002. Pyroclastic flows generated by crater-wall collapse and outpouring of the lava pool of Arenal Volcano, Costa Rica. *Bull. Volcanol.* 63 (8), 557–568.
- Arellano, S., Hall, M., 2007. Velocidades de emisión de bombas expulsadas por el volcán Tungurahua el 16–17 de agosto de 2006. *Memorias 6th Jorn. Cien. Tierra, Esc. Poli. Nac. Quito*, pp. 185–188.
- Arellano, S., Hall, M., Samaniego, P., Le Pennec, J.-L., Ruiz, A., Molina, I., Yepes, H., 2008. Degassing patterns of Tungurahua volcano (Ecuador) during the 1999–2006 eruptive period, inferred from remote spectroscopic measurements of SO_2 emissions. *J. Volcanol. Geotherm. Res.* 176, 151–162.
- Babrauskas, V., 2001. Ignition of Wood: A Review of the State of the Art. *Interflam. Interscience Communications Ltd., London*, pp. 71–88.
- Barba, D., Arellano, S., Ramón, P., Mothes, P., Alvarado, A., Ruiz, G., Troncoso, L., 2006. Cronología de los eventos eruptivos de Julio y Agosto del 2006 del volcán Tungurahua. *Memorias 6th Jorn. Cien. Tierra, Esc. Poli. Nac. Quito*, pp. 177–180.
- Café, A.D., 2007. Physical Constants for Investigators, T.C. Forensic Web Page.
- Cashman, K., Sturtevant, B., Papale, P., Navon, O., 2000. Magmatic fragmentation. In: Sigurdsson, H. (Ed.), *Encyclopedia of Volcanoes*. Academic Press, New York, pp. 421–430.
- Cioni, R., Marianelli, P., Santacroce, R., Sbrana, A., 2000. Plinian and subplinian eruptions. In: Sigurdsson, H. (Ed.), *Encyclopedia of Volcanoes*. Academic Press, New York, pp. 477–494.
- Cole, P.D., Calder, E.S., Sparks, R.S.J., Clarke, A.B., Druitt, T.H., Young, S.R., Herd, R.A., Harford, C.L., Norton, G.E., 2002. Deposits from dome-collapse and fountain-collapse pyroclastic flows at Soufriere Hills Volcano, Montserrat. In: Druitt, T.H., Kokelaar,

- B.P. (Eds.), The eruption of Soufriere Hills Volcano, Montserrat, from 1995 to 1999. *Geol Soc London Mem*, 21, pp. 231–262.
- Cole, P.D., Fernandez, E., Duarte, E., Duncan, A.M., 2005. Explosive activity and generation mechanisms of pyroclastic flows at Arenal volcano, Costa Rica between 1987 and 2001. *Bull. Volcanol.* 67, 695–716.
- Douillet, G., Pacheco, D.A., Goldstein, F., Tsang-Hin-Sun, E., Kueppers, U., Hanson, J.B., Bustillos, J., Robin, C., Dingwell, D.B., 2010. Volcaniclastic dunes from the 2006 deposits of Tungurahua volcano, Ecuador. Poster V13A-2344, AGU Fall Mtg 2010, San Francisco.
- Druitt, T.H., Young, S.R., Baptie, B., Bonadonna, C., Calder, E.S., Clarke, A.B., Cole, P.D., Harford, C.L., Herd, R.A., Luckett, R., Ryan, G., Voight, B., 2002. Episodes of cyclic Vulcanian explosive activity with fountain collapse at Soufriere Hills Volcano, Montserrat. In: Druitt, T.H., Kokelaar, B.P. (Eds.), The eruption of Soufriere Hills Volcano, Montserrat, from 1995 to 1999. *Geol Soc London Mem*, 21, pp. 281–306.
- Eycheenne, J., Le Pennec, J.-L., Troncoso, L., Gouhier, M., Nedelec, J.-M., 2012. Causes and consequences of bimodal grain-size distribution of tephra fall deposited during the August 2006 Tungurahua eruption (Ecuador). *Bull. Volcanol.* <http://dx.doi.org/10.1007/s00445-011-0517-5>.
- Fee, D., Garcés, M., Steffke, A., 2010. Infrasonic from Tungurahua volcano 2006–2008: Strombolian to Plinian activity. *J. Volcanol. Geotherm. Res.* 193, 67–81.
- Garcés, M., Fee, D., McCormack, D., Servranckx, R., Bass, H., Hetzer, C., Hedlin, M., Matoza, R., Yepes, H., Ramon, P., 2008. Capturing the acoustic fingerprint of stratospheric ash injection. *Eos. Trans. AGU* 89 (40), 377–379.
- Hall, M., Robin, C., Beate, B., Mothes, P., Monzier, M., 1999. Tungurahua volcano, Ecuador: structure, eruptive history and hazards. *J. Volcanol. Geotherm. Res.* 91, 1–21.
- Hall, M.L., Robin, C., Samaniego, P., Monzier, M., Eissen, J., Mothes, P., Yepes, H., 2002. Mapa de Los Peligros Potenciales del Volcán Tungurahua, Ecuador. Instituto Geofísico, Esc. Pol. Nac. Quito. Escala 1:50,000.
- Hall, M.L., Samaniego, P., Le Pennec, J.-L., Johnson, J.B., 2008. Ecuadorian Andes volcanism: a review of late Pliocene to present activity. *J. Volcanol. Geotherm. Res.* 176, 1–6.
- Hanson, J.B., Lavallée, Y., Hess, K.U., von Aulock, F.W., Dingwell, D.B., 2009. Rheology of the 2006 eruption at Tungurahua volcano, Ecuador. *Geophys. Res. Abstr.* 11, EGU2009–EGU10171.
- Johnson, J.B., Ripepe, M., 2011. Volcano infrasonic: a review. *J. Volcanol. Geotherm. Res.* 206 (3–4), 61–69.
- Kelfoun, K., Samaniego, P., Palacios, P., Barba, D., 2009. Testing the suitability of frictional behaviour for pyroclastic flow simulation by comparison with a well-constrained eruption at Tungurahua volcano (Ecuador). *Bull. Volcanol.* 71, 1057–1075.
- Kumagai, H., Nakano, M., Maeda, T., Yepes, H., Palacios, P., Ruiz, M., Arrais, S., Vaca, M., Molina, I., Yamashita, T., 2010. Broadband seismic monitoring of active volcanoes using deterministic and stochastic approaches. *J. Geophys. Res.* 115, B08303. <http://dx.doi.org/10.1029/2009JB006889>.
- Le Pennec, J.-L., Jaya, D., Samaniego, P., Ramón, P., Moreno, S., Egred, J., van der Plicht, J., 2008. The AD 1300–1700 eruptive periods at Tungurahua volcano, Ecuador, revealed by historical narratives, stratigraphy, and radio-carbon dating. *J. Volcanol. Geotherm. Res.* 176, 70–81.
- Marchetti, E., Ripepe, M., Harris, A.J.L., Delle Donne, D., 2009. Tracing the differences between Vulcanian and Strombolian explosions using infrasonic and thermal radiation energy. *Earth Planet. Sci. Lett.* 279, 273–281.
- McNutt, S., Tytgat, G., Estes, S., Stihler, S., 2010. A parametric study of the January 2006 explosive eruptions of Augustine volcano, using seismic, infrasonic, and lightning data. In: Power, J.A., Coombs, M.L., Freymueller, J.T. (Eds.), The 2006 eruption of Augustine Volcano, Alaska. USGS Prof. Paper, 1769, pp. 85–104.
- Miller, T.P., Neal, C.A., Waitt, R.B., 1995. Pyroclastic flows of the 1992 Crater Peak eruptions: distribution and origin. In: Keith, T.E. (Ed.), The 1992 eruptions of Crater Peak Vent, Mount Spurr Volcano, Alaska. U.S. Geological Survey Bull., 2139, pp. 81–87.
- Miyabuchi, Y., Watanabe, K., Egawa, Y., 2006. Bomb-rich basaltic pyroclastic flow deposit from Nakadake, Aso Volcano, southwest Japan. *J. Volcanol. Geotherm. Res.* 155, 90–103.
- Morrissey, M.M., Mastin, L.G., 2000. Vulcanian eruptions. In: Sigurdsson, H. (Ed.), *Encyclopedia of Volcanoes*. Academic Press, New York, pp. 463–475.
- Mothes, P., Hall, M., Samaniego, P., Ramón, P., Molina, I., Yepes, H., Le Pennec, J.-L., Ruiz, G., Andrade, D., Enriquez, W., Garcia, A., Eissen, J.-P., Hidalgo, S., Monzier, M., 2004. Monitoring of a drawn-out episodic eruption. Tungurahua Abstract, Cities on Volcanoes, 5 (Pucón, Chile).
- Petersen, E.T., De Angelis, S., Tytgat, G., McNutt, S.R., 2006. Local infrasonic observations of large ash explosions at Augustine Volcano, Alaska, during January 11–28, 2006. *Geophys. Res. Lett.* 33, L12303. <http://dx.doi.org/10.1029/2006GL026491>.
- Pierson, T.C., 1985. Initiation and flow behavior of the 1980 Pine Creek and Muddy River lahars, Mount St. Helens, Washington. *Bull. Geol. Soc. Am.* 96, 1056–1069.
- Ruiz, M., Lees, J.M., Johnson, J.B., 2006. Source constraints of Tungurahua volcano explosion events. *Bull. Volcanol.* 68, 480–490.
- Samaniego, P., Le Pennec, J.-L., Robin, C., Hidalgo, S., 2011. Petrological analysis of the pre-eruptive magmatic process prior to the 2006 explosive eruptions at Tungurahua volcano, Ecuador. *J. Volcanol. Geotherm. Res.* 199, 69–84.
- Steffke, A.M., Fee, D., Garcés, M., Harris, A., 2010. Eruption chronologies, plume heights and eruption styles at Tungurahua volcano: integrating remote sensing techniques and infrasonic. *J. Volcanol. Geotherm. Res.* 193, 143–160.
- Troncoso, L., Le Pennec, J.-L., Jaya, D., Vallee, A., Mothes, P., Arrais, S., 2006. Depósitos de caída de ceniza producidos durante las erupciones del volcán Tungurahua, 14 de Julio y 16 de Agosto de 2006. *Memorias 6th Jorn. Cien. Tierra, Esc. Poli. Nac. Quito*, pp. 181–184.
- Vallance, J.W., Bull, K.F., Coombs, M.L., 2010. Pyroclastic flows, lahars, and mixed avalanches generated during the 2006 eruption of Augustine Volcano. In: Power, J.A., Coombs, M.L., Freymueller, J.T. (Eds.), The 2006 eruption of Augustine Volcano, Alaska. USGS Prof. Paper, 1769, pp. 219–267.
- Wright, H.M., Cashman, K.V., Rosi, M., Cioni, R., 2007. Breadcrust bombs as indicators of Vulcanian eruption dynamics at Guagua Pichincha volcano, Ecuador. *Bull. Volcanol.* 69, 281–300.
- Wright, H.M., Cashman, K.V., Mothes, P.A., Hall, M.L., Ruiz, A.G., Le Pennec, J.-L., 2012. Estimating rates of decompression from textures of erupted ash particles produced by 1999–2006 eruptions of Tungurahua volcano, Ecuador. *Geology* 40, 619–622.